

Mechanistic Understanding of the Interactions and Pseudocapacitance of Multi-Electron Redox Organic Molecules Sandwiched between MXene Layers

Muhammad Boota,* Tanveer Hussain, Long Yang, Matthieu Bécuwe, William Porzio, Luisa Barba, and Rajeev Ahuja

Using a combined theoretical and experimental approach, a mechanistic understanding of the interactions and pseudocapacitance of different quinone-coupled viologen and pyridinium molecules sandwiched between titanium carbide ($\text{Ti}_3\text{C}_2\text{T}_x$) MXene layers has been provided. Three different derivatives of quinone-coupled viologen and pyridinium are synthesized using nucleophilic substitution reaction and subsequently hybridized with $\text{Ti}_3\text{C}_2\text{T}_x$ MXene ($\text{organic@Ti}_3\text{C}_2\text{T}_x$) using self-assembly approach. The atomic structure of pristine $\text{Ti}_3\text{C}_2\text{T}_x$ and $\text{organic@Ti}_3\text{C}_2\text{T}_x$ hybrid films is investigated using grazing incidence X-ray diffraction and X-ray pair distribution function analysis using synchrotron radiation. Spectroscopic results confirm the coupling of quinones with viologen and pyridinium molecules and their non-covalent functionalization to the MXene without their catalytic decomposition. First-principles calculations confirm that the preferred orientation of organic molecules upon intercalation/adsorption is horizontal to the $\text{Ti}_3\text{C}_2\text{T}_x$ surface. The authors reveal that these molecules attach to the $\text{Ti}_3\text{C}_2\text{T}_x$ surface with a significantly high binding energy (up to -2.77 eV) via a charge transfer mechanism. The electronic structure calculations show that all $\text{organic@Ti}_3\text{C}_2\text{T}_x$ hybrids preserved their metallic behavior. Free-standing $\text{organic@Ti}_3\text{C}_2\text{T}_x$ hybrid films show a more than three times higher capacitance at ultra-high scan rates (up to 20 V s^{-1}) compared to their pristine counterpart due to molecular pillaring of organic molecules between $\text{Ti}_3\text{C}_2\text{T}_x$ layers via strong binding energies and charge transfer.


1. Introduction

Since the discovery of the $\text{Ti}_3\text{C}_2\text{T}_x$ MXene, the family of MXene materials has seen a dramatic growth ranging from their innovative synthesis to surface modifications to a wide range of applications.^[1] MXenes are 2D transition metal carbides, nitrides, and carbonitrides that are represented with a general formula of $M_{n+1}X_nT_x$ ($M = \text{Ti, Mo, Nb, V}$; X is C and/or N; $T_x = \text{O, OH, F, and/or Cl}$; and $n = 1, 2, \text{ or } 3$).^[2] Unlike other 2D materials, MXenes offer a unique set of properties including hydrophilicity, metallic conductivity, redox performance, a greater range of chemical compositions (>30 MXenes reported), high mechanical strength (Young's modulus ≈ 330 GPa), ease of processability (powder, free-standing films, fibers, printing, writing, coating, and so forth), and scalability, which altogether are rare to find in any known 2D material.^[1,2] These properties enable their use in electromagnetic interference (EMI) shielding, energy conversion and storage, sensors, catalysis, separation membranes,

Dr. Md. Boota
A. J. Drexel Nanomaterials Institute and Department of Materials
Science and Engineering
Drexel University
Philadelphia 19104, PA
E-mail: boota@drexel.edu

Dr. T. Hussain
School of Molecular Sciences
The University of Western Australia
Perth, WA 6009, Australia

Dr. T. Hussain
School of Chemical Engineering
The University of Queensland, St Lucia
Brisbane 4072, Australia

 The ORCID identification number(s) for the author(s) of this article can be found under <https://doi.org/10.1002/aelm.202001202>.

Dr. L. Yang
Department of Applied Physics and Applied Mathematics
Columbia University
New York, NY 10027

Prof. M. Bécuwe
Laboratoire de Réactivité et Chimie des Solides (LRCS), UMR CNRS 7314
Université de Picardie Jules Verne (UPJV)
33 rue Saint Leu, Amiens 80039, France

Prof. M. Bécuwe
Institut de Chimie de Picardie (ICP), CNRS FR3085
Université de Picardie Jules Verne
Amiens Cedex 80039, France

Prof. M. Bécuwe
Réseau sur le Stockage Electrochimique de l'Energie (RS2E)
FR CNRS, 3459, France

DOI: 10.1002/aelm.202001202

antimicrobial, optoelectronics, composites/hybrids, and biomedical applications.^[1–5]

To further expand the scope of the MXene research, MXenes have been combined with organic molecules, and polymers to manufacture MXene–organic composites/hybrids.^[6] Organic materials have offered multifunctional roles in these hybrids such as intercalation and delamination of the MXene layers,^[7] improved electrochemical performance,^[8] served as the nano-fillers to improve mechanical characteristics,^[2] improved the EMI shielding performance,^[3] and so forth.^[1,2] The combination of the organic materials with MXenes has improved the performance of the hybrids due to the synergistic impact of the MXenes.^[1–5] However, the challenge that remained is the fundamental understanding of interaction chemistry at heterointerfaces and how to effectively control them.^[9] While terminations of the MXenes are useful for a variety of applications^[1,2,4,5] they impose a great challenge to control the MXene–organic interfacial chemistry. These terminations are extremely reactive and interact abruptly with organic molecules.^[9,10] Therefore, the full potential of MXene–organic hybrid materials may not be fully achieved if interactions at MXene–organic heterointerfaces are poorly understood.

Previously, we have seen that a simple room temperature mixing of the $Ti_3C_2T_x$ MXene with organic molecules of varying end-groups (O, S, N, secondary amines) involved a variety of complex interactions between $Ti_3C_2T_x$ MXene and organic molecules such as electrostatic interactions, polymerization, strong binding, and in some cases catalytic decomposition of the organic molecules.^[9] We have also shown that $Ti_3C_2T_x$ MXene prefers to interact with the positively charged nitrogen-containing polymers compared to their nonpolar/uncharged counterparts via weak physical interactions.^[11] Furthermore, we have reported that monomers of conducting polymers such as pyrrole and 3,4-ethylenedioxythiophene (EDOT) spontaneously convert into their polymeric forms when mixed with $Ti_3C_2T_x$ MXene in absence of any oxidant.^[8,12] Gang et al. recently reported that dopamine follows a similar path to pyrrole and EDOT, and transforms into polydopamine.^[13] Steven et al. found that urea molecules decompose readily upon mixing with the $Ti_3C_2T_x$ MXene solution, and the decomposed ammonium cations intercalate between MXene layers along with evolving carbon dioxide.^[14] It has also been shown that mixing

of the glycine with $Ti_3C_2T_x$ yields covalent attachment of the glycine molecules to the $Ti_3C_2T_x$ surface.^[15] These examples clarify that MXene interacts with organic molecules rapidly and in most cases in an uncontrolled fashion involving a variety of complex interactions, therefore, making it difficult to generalize interaction chemistries of the MXenes and organic molecules. This poses a challenge to further explore and understand the fundamental interaction mechanisms of organic molecules with different MXenes.

Among nearly unlimited organic molecules, multi-electron redox organic molecules are attractive for a range of applications including electrochemical energy storage, water purification, sensors, biomedical applications, and so forth.^[16] Development of innovative organic molecules and understanding their interaction chemistries at MXene–organic heterointerfaces may guide the manufacturing of new organic–inorganic hybrid materials with defined architectures, properties, and applications. Viologen/pyridinium and quinone compounds are of interest due to their fast kinetics of one and two electron exchange, respectively.^[17,18] We hypothesized that quinone molecules can be coupled with viologen and pyridinium molecules to synthesize multi-electron redox organic molecules which can be of interest for a range of applications where redox reactions are critically needed. These molecules can further be hybridized with MXenes to gain the benefits of MXenes such as high mechanical strength, excellent conductivity, electrochemical redox, to name just a few.^[1–5]

Herein, we provide a simple synthesis approach to produce multi-electron redox quinone-coupled viologen and pyridinium derivatives followed by their hybridization with the $Ti_3C_2T_x$ MXene using a self-assembly approach. Intercalation, interaction chemistry, atomic structure, and charge storage performance are investigated using combined experimental and computational methods.

2. Results and Discussion

Figure 1 shows the schematic of the synthesis of the quinone-coupled viologen and pyridinium derivatives. Our idea was to produce hybrid organic materials that could utilize the redox centers of the quinones, viologen, and pyridinium. By simple mixing at room temperature, viologens, or pyridiniums were coupled to quinone molecules using quaternization reaction in which nitrogen-free doublet attacks carbon-bearing chlorine atom (nucleophilic substitution reaction). Using this approach, three derivatives (**Figure 1**) were synthesized namely *C1* (2-pyridin-1-ium-1-yl-1,4-benzoquinone chloride), *C2* (2,5-di(pyridin-1-ium-1-yl)-1,4-benzoquinone chloride), and *C3* (1,1-di(1,4-benzoquinonyl)-4,4'-bipyridinium chloride). These molecules were further combined with $Ti_3C_2T_x$ suspensions in a 1:2 weight ratio, mixed overnight, and filtered to get free-standing films that were used for the further characterizations (see Supporting Information for more details).

XRD analysis confirmed the intercalation/adsorption of the organic molecules between $Ti_3C_2T_x$ layers. XRD patterns (**Figure 2a**) of the pristine $Ti_3C_2T_x$ MXene and organic@ $Ti_3C_2T_x$ hybrids showed significant expansion of the c-LP, confirmed by the second-order (002) diffraction peaks. The highest expansion

Dr. W. Porzio
Institute of Chemical Sciences and Technologies “G.Natta” Consiglio Nazionale delle Ricerche (SCI-TEC) via
A. Corti 12, Milano 20133, Italy

Dr. L. Barba
Istituto di Cristallografia del CNR-Sincrotrone Elettra
Strada Statale 14-Km 163, 5 Area Science Park, Basovizza, Trieste 34149, Italy

Prof. R. Ahuja
Condensed Matter Theory Group
Department of Physics and Astronomy, Box 516
Uppsala University
Uppsala S-75120, Sweden

Prof. R. Ahuja
Applied Materials Physics
Department of Materials and Engineering
Royal Institute of Technology, (KTH)
Stockholm S-100 44, Sweden

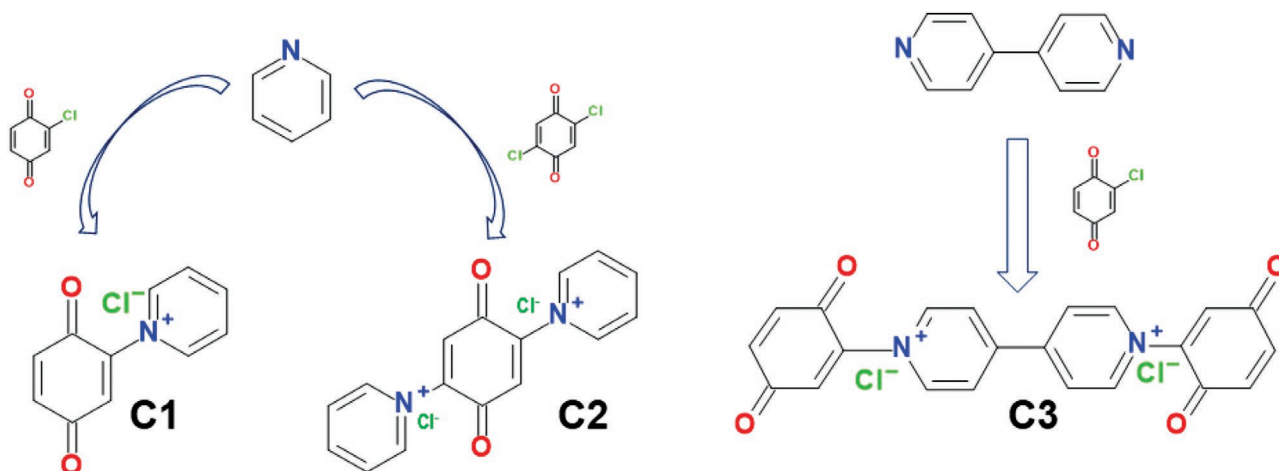


Figure 1. Synthesis scheme of the quinone-coupled viologen and pyridinium derivatives. The proposed redox reactions are shown in Scheme S1, Supporting Information.

of the *c*-axis was noticed for the C1@Ti₃C₂T_x hybrid film from 24.88 Å (Ti₃C₂T_x) to 44.24 Å, showing remarkable expansion (≈20 Å) of Ti₃C₂T_x layers. This *c*-axis increase allows the insertion of at least three molecules among adjacent inorganic layers (Figure 2b) or also two molecules bent inserted into the Ti₃C₂T_x channels. The expansion of the *c*-axis was slightly lower (≈17 Å) for the C2@Ti₃C₂T_x hybrid film. For C3@Ti₃C₂T_x hybrid film, the *c*-LP expansion was the lowest (≈14 Å). This *c*-LP expansion

corresponds to the insertion of only two stacked molecules in any achievable configuration (Figure 2c).

Organic@Ti₃C₂T_x hybrid films were further investigated by grazing incidence XRD (GIWAXS) using synchrotron radiations. We have shown 2D images in Figure 2d–f and extracted out-of-plane (OOP) and in-plane (IP) profiles are given in Figures S1 in which the indexing of the key diffraction arcs is given. In C1@Ti₃C₂T_x hybrid film, six orders of [00l] although

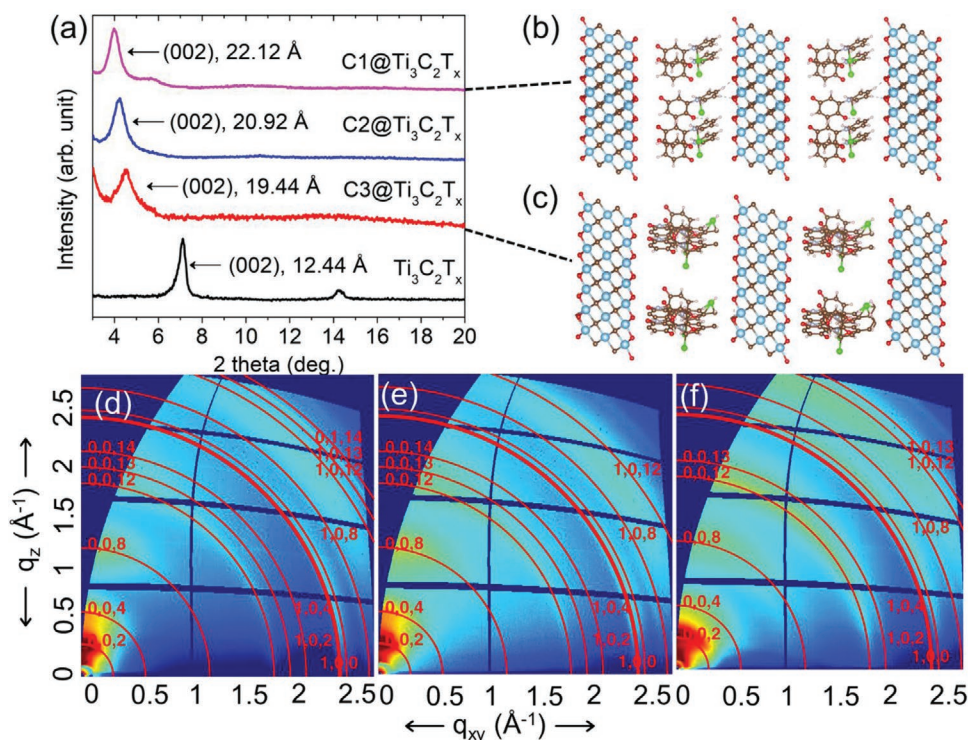


Figure 2. a) XRD patterns of pristine Ti₃C₂T_x MXene and investigated C1/C2/C3-containing hybrids. b) Model of C1@Ti₃C₂T_x hybrid with three stacked molecules inserted into adjacent inorganic layers, as viewed along (110) diagonal in the pseudo-hexagonal cell approximation. c) Model of C3@Ti₃C₂T_x hybrid, with two molecules in a bent conformation as viewed along (110) diagonal in the pseudo-hexagonal cell approximation. GIDVis 2D, *q*-space indexed images from DECTRIS detector of films of d) C1@Ti₃C₂T_x, e) C2@Ti₃C₂T_x, and f) C3@Ti₃C₂T_x. The colors are not representative of the intensity scale in OOP and IP profiles in Figure S1, Supporting Information, where LP, geometry, pixel distance and detector efficiency corrections applied.

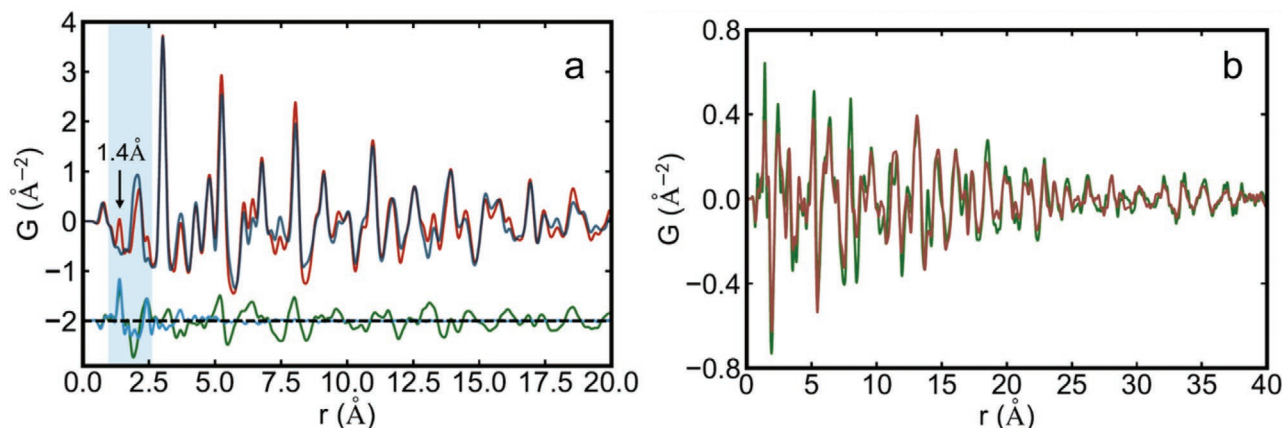


Figure 3. a) The PDFs of C1@Ti₃C₂T_x (red) and pristine Ti₃C₂T_x MXene (dark blue) are plotted together on the top, and their difference curve is shown in the bottom in green. The experimental PDF of C1 sample is shown in light blue curve offset below together with the residual signal. b) The difference PDFs of C1@Ti₃C₂T_x and C3@Ti₃C₂T_x subtracting the pristine Ti₃C₂T_x MXene are plotted in green and brown curves, respectively.

not perfectly registered are clearly detected in OOP, while in IP an evident (100) emerges, hence a good orientation along the *c*-axis is constantly preserved (Figure 2d, Figure S1a). The same considerations can be applied to the case of the C2@Ti₃C₂T_x hybrid, namely unregistered five orders of [00l] in OOP along with (100) peak in IP profiles, as shown in Figure S1b. The profiles of C3@Ti₃C₂T_x hybrid film are reported in Figure S1c. Six orders of the same crystallographic direction can be recognized, the presence of (100) reflection both in IP and OOP profiles maps an incomplete orientation of hybrid crystals normal to the film plane. In all cases, odd 00L reflections are found, mapping the decrease of the hexagonal symmetry, for example, from P6₃, observed in pure Ti₃C₂T_x, to P6. We expanded the profile in logarithmic scale to evidence weaker peaks in Figure S1. In the latter, it is possible to observe the much lesser orientation of C3@Ti₃C₂T_x, testified by the presence of (100) in OOP profiles.

To obtain more quantitative atomic structure information of the organic@MXenes, the X-ray atomic pair distribution function (PDF) analysis was performed. The PDF gives the scaled probability of finding two atoms in a material a distance *r* apart and is related to the density of atom pairs in the material.^[19] The technique does not presume periodicity, so it is well suited for studying structures of many advanced materials, especially when they are nanostructured.^[20–22] To study how the structure changes after the intercalation, we first subtracted the C1@Ti₃C₂T_x PDF from the pristine MXene, and the residual is plotted in the green curve in Figure 3a. There is an evident intercalation-induced structural change over the low-*r* region. The 1.4 Å PDF peak can be found in the C1@Ti₃C₂T_x data but not in the pristine Ti₃C₂T_x MXene, which is contributed from the C–C and C–N bonds in the C1 organic compound. The intra-layer structure is approximately considered as the summation of Ti₃C₂T_x and C1 compounds, since the residual signal after subtracting the pristine Ti₃C₂T_x MXene matches reasonably well with the measured PDF of C1 compound over the low-*r* region, as shown in green and light blue curves, respectively, over the highlighted shaded region in the bottom of Figure 3a.

A similar change of the local structure when intercalating C3 into Ti₃C₂T_x MXene is also observed for the C3@Ti₃C₂T_x sample (see Figure S2). In the high-*r* region, obviously, the

residuals from different organics are quite similar, as shown in Figure 3b. This indicates that the Ti₃C₂T_x MXene inter-layer structure is changed in the same way for different organics. It is possible that the intercalation of organics can further increase turbostratic disordering from the pristine Ti₃C₂T_x MXene, as found in other organic@MXene systems by comparing the inter-layer correlation and experimental signal residual.^[9] Thus, the intercalation of the organics may remove any residual stacking order that has existed in the pristine Ti₃C₂T_x MXene,^[23] as already pointed out in the XRD discussion.

Figures 4a and b show the transmission electron microscopy (TEM) images of the C2@Ti₃C₂T_x MXene flake and the cross-sectional TEM image of C2@Ti₃C₂T_x, respectively. Visibly, Ti₃C₂T_x flakes are covered with the C2 organic molecules (Figure 4a, S5), and those molecules are also confined and aligned between 2D Ti₃C₂T_x MXene layers (Figure 4b).

The Fourier-transform infrared (FTIR) spectra of organic@MXene are shown in Figure 4c–e. The C1@Ti₃C₂T_x and C2@Ti₃C₂T_x showed several common bands. The band at 1625 cm^{−1} is due to C=C stretching in both hybrids.^[9] The strong bands at 1554 and 1469 cm^{−1} are assigned to the vibrations of coupled pyridinium molecules.^[24,25] The bands at 1420 and 1345 cm^{−1} show the coupling of the pyridinium to carbonyl-containing reactants.^[25–27] The bands at 1263, 1191, 1020, 824, 776, and 680 cm^{−1} are assigned to C–Cl vibrations, C–H bending vibrations, pyridinium ring vibrations, C–H out of plane bending vibrations, ring deformation, and coupled pyridinium associated vibrations, respectively.^[28,29] The bands in C3@Ti₃C₂T_x spectrum at 1558 and 1485 cm^{−1} confirm the vibrations of bipyridinium and the strong one at 815 cm^{−1} shows in-plane bending frequency of substituted dipyrindyl.^[30,31] The symmetric vibrations of C–N can be associated with bands at 1405, 1370, and 1341 cm^{−1}.^[9,32] The bands at 1634 and 1433 cm^{−1} can be ascribed to C=C stretching mode and C–H bending vibrations, respectively.^[32,33] Furthermore, bands at 1248, 1204, and 1139 cm^{−1} are associated with the coupled bipyridine.^[34] The bands at 786, 720, and 668 cm^{−1} are associated with the C–H out-of-plane ring deformation, C–H bending, and C–O vibrations.^[35] It is important to mention that the FTIR spectrum of the pristine Ti₃C₂T_x appears featherless in the tested regime.^[11]

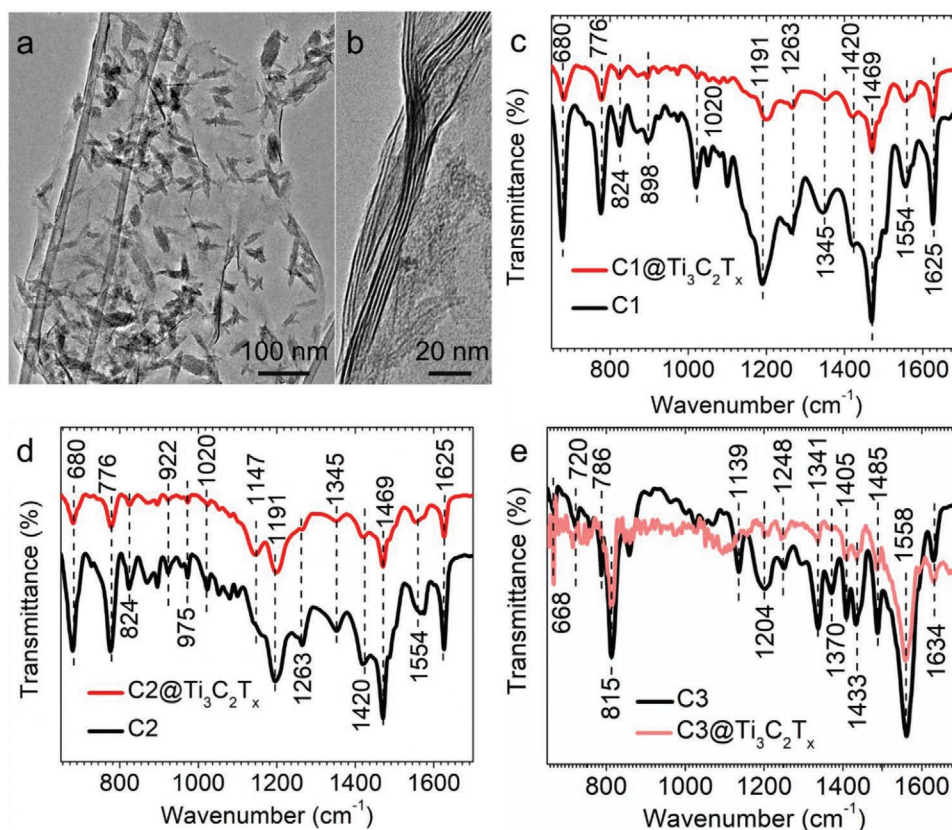


Figure 4. a,b) TEM images display that $\text{Ti}_3\text{C}_2\text{T}_x$ MXene flakes are covered with the C2 molecules (a) and the $\text{C2@Ti}_3\text{C}_2\text{T}_x$ hybrid consists of confined and aligned C2 organic molecules (bright layers). FTIR spectra of c) $\text{C1@Ti}_3\text{C}_2\text{T}_x$, d) $\text{C2@Ti}_3\text{C}_2\text{T}_x$, and e) $\text{C3@Ti}_3\text{C}_2\text{T}_x$.

All three organic molecules showed sharp bands that are typically observed for the organic molecules. FTIR spectra of all hybrids did not show any blue or redshift. Qualitatively, this confirms three important findings: 1) organic molecules interact with the $\text{Ti}_3\text{C}_2\text{T}_x$ layers via non-covalent interactions. $\text{Ti}_3\text{C}_2\text{T}_x$ MXene contains $-\text{OH}$, $-\text{O}$, $-\text{F}$, and $-\text{Cl}$ surface functional groups which are the key modulator for the surface-driven interactions with organic molecules.^[9] As all investigated organic molecules contain carbonyl end-groups and nitrogen in their core, it is very likely that these groups potentially interacted with the surface groups of $\text{Ti}_3\text{C}_2\text{T}_x$ MXene via hydrogen bonding;^[9,15] 2) the positive charge of the pyridinium/bipyridinium rings will induce strong electrostatic coupling with the negatively charged surface of the $\text{Ti}_3\text{C}_2\text{T}_x$ yielding fully functional interfaces;^[11] and 3) the molecular structure of these organic molecules stayed intact and did not transform into any polymeric form due to catalytic behavior of the $\text{Ti}_3\text{C}_2\text{T}_x$ MXene. It is important to mention that $\text{Ti}_3\text{C}_2\text{T}_x$ MXene reacts strongly with the organic molecules due to the strong catalytic character of the MXene surface (see examples in the introduction and references).^[8,9,11,12,14,15] To the best of our knowledge, there is no rule of thumb to describe the MXene interactions with a broad set of organic molecules and that is where the complexity arises. Here, we have noticed that despite having charged nitrogen in the core of the organic molecules, we did not observe the dissociation of investigated organic molecules. This may be ascribed to the presence of carbonyl end-groups which tend to be the

least reactive to initiate the chemical reaction with the MXene surface functionalities.^[9] Therefore, to have better control on the MXene–organic hybrid interface and thus properties, it is important to design organic molecules having end-groups that do not take part in the catalytic decomposition/transformation of the organic molecules on reactive MXene surfaces. Better control on organic@MXene properties can be achieved if they exhibit weak physical interactions (e.g., hydrogen bonding, van der Waals forces, and/or π – π interactions), or chemically grafted in such a way that inhibit the catalytic transformation of the organic molecules into other products as seen in previous studies.^[8,9,11,12,14,15]

Brief structural properties of $\text{Ti}_3\text{C}_2\text{O}_2$ were presented before exploring its binding and charge transfer mechanism towards incident organic species, C1, C2, and C3. We used a $4 \times 4 \times 1$ supercell of $\text{Ti}_3\text{C}_2\text{O}_2$, consisting of 112 atoms, ($\text{Ti} = 48$, $\text{C} = \text{O} = 32$) and found it large enough to accommodate the organic molecules. Optimized Ti–C and Ti–O bond lengths were calculated as 2.15 and 1.97 Å, respectively, which agreed well with the literature.^[5,36] The optimized structures of the $\text{Ti}_3\text{C}_2\text{O}_2$ and C1, C2, and C3 are given in Figure S3. In pursuit of attaining the most stable binding configurations of organic molecules C1, C2, and C3 over $\text{Ti}_3\text{C}_2\text{O}_2$, the former was introduced at all available binding sites over the surface of the latter. Furthermore, different orientations of the organic molecules were also considered to explore the lowest energy structures. It is important to mention here that several initial configurations were

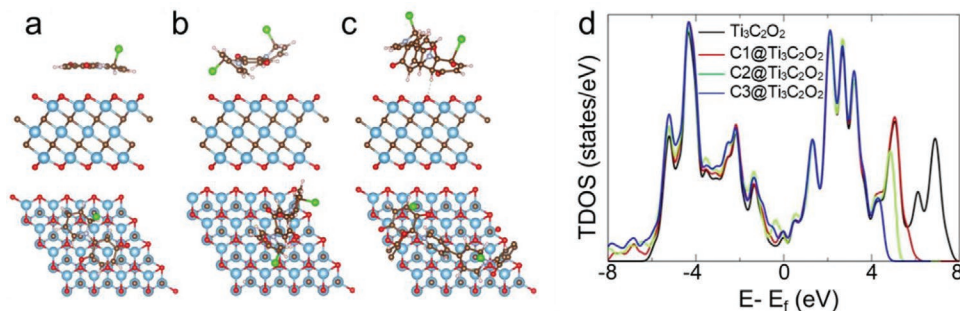


Figure 5. Optimized structures of the top and side views of a) C1@Ti₃C₂O₂, b) C2@Ti₃C₂O₂, and c) C3@Ti₃C₂O₂. Blue, brown, red, green, and pink balls represent Ti, C, O, Cl, and H atoms, respectively. d) Electronic properties of pristine and doped Ti₃C₂O₂ through plotting their density of states plots show that all the hybrids preserved metallic character.

considered for the parallel and horizontal configurations of the organic molecules. The binding energies (E_b) were calculated by using the following relation,

$$E_b = E(\text{Ti}_3\text{C}_2\text{O}_2 @ \text{C}_y) - E(\text{Ti}_3\text{C}_2\text{O}_2) - E(\text{C}_y) \quad (1)$$

$(\text{C}_y = \text{C1, C2, and C3})$

In the above relation, the first, second, and third terms represent the total energies of Ti₃C₂O₂ doped with organic molecules, pristine Ti₃C₂O₂, and the organic molecules, respectively. The energetic analysis showed strong E_b values of -1.37 , -1.61 , and -2.77 eV for C1, C2, and C3, respectively in their horizontal configurations (Figure 5a–c). A lower E_b value (more negative number) corresponded to a stronger binding mechanism. Based on this definition, we found that the order of binding of the incident organic molecules (with Ti₃C₂O₂) was C3 > C2 > C1. The minimum binding distances (Δd) of C1, C2, and C3 with Ti₃C₂O₂ were found as 3.06, 2.20, and 2.08 Å, respectively. For comparison, we calculated the E_b values of the organic molecules in their vertical configurations over Ti₃C₂O₂ (Figure S4) which yielded a comparatively lower E_b of -0.75 , -1.30 , and -1.62 eV for C1, C2, and C3, respectively.

To gain an insight into the origin of the strong binding mechanism between Ti₃C₂T_x and organic molecules (horizontal configurations), we performed a charge analysis. We found that all the organic molecules transfer a significant amount of charges to the Ti₃C₂O₂. A precise analysis revealed that 1.11, 1.27, and 2.60 electrons were transferred by C1, C2, and C3, respectively. This clearly indicated that the higher the transferred charge from the organic molecule, the stronger was its binding with Ti₃C₂O₂. Finally, we discussed the electronic properties of pristine and doped Ti₃C₂O₂ by plotting their density of states (TDOS) plots (Figure 5d). From the TDOS plots, it was evident that all hybrids preserved a metallic character.

Multi-electron redox organic materials offer the potential to boost the charge storage performance of the supercapacitors.^[18] Ti₃C₂T_x MXene is well-known for its high capacitance ($\approx 1500 \text{ F cm}^{-3}$, 450 F g^{-1}).^[4] For electrochemical analysis of the hybrid electrodes, our aim here was to further stretch the limits of the Ti₃C₂T_x MXene capacitance by hybridization with multi-electron redox molecules and to further understand the MXene interface when combined with these organic systems. Using cyclic voltammetry (CV), we investigated the pseudocapacitance

of the organic@MXene (C1/C2/C3) hybrid films ($\approx 6\text{--}8 \mu\text{m}$) in a 3-electrode configuration in 3 M H₂SO₄. All three hybrids exhibited pseudocapacitive character obvious from the narrow redox peak separations (Figure 6a–c).^[37] C1 and C2-containing hybrids showed a single redox peak centered at ≈ -0.3 V (Figure 6a,b), whereas, C3-containing hybrid showed a pair of the redox peaks centered at ≈ -0.35 and ≈ 0.2 V (Figure 6c) likely due to additional carbonyl ends.

Ti₃C₂T_x MXene film exhibited the higher capacitance at low scan rates ($10\text{--}100 \text{ mV s}^{-1}$), while the trend appeared opposite at higher scan rates (Figure 6d) which can be ascribed to the stacking of the Ti₃C₂T_x MXene sheets.^[38] All hybrids showed higher capacitance above 100 mV s^{-1} compared to their pristine counterpart. For instance, C2@Ti₃C₂T_x showed more than 3.5 times higher capacitance at an ultra-high scan rate of 2 V s^{-1} (43 versus 151 F g^{-1}), and the difference was even higher at higher scan rates (Figure 6d inset). The high capacitance of these hybrids, particularly C2@Ti₃C₂T_x hybrids, at ultra-high scan rates confirms that organic molecules served as the molecular spacers which expanded the interlayer spacing (Figure 2) and allowed facile ionic and electronic transport.^[10] Among the three hybrids, C2@Ti₃C₂T_x showed the highest capacitance and shallower drop in capacitance at ultra-high scan rates ($>0.5 \text{ V}$). This is likely because the redox-active centers in C2 molecules are protected and are less prone to potential-induced dissolution and degradation compared to C1 and C3 molecules.^[39] Another aspect to note here is that Ti₃C₂T_x MXene interface behaved opposite to carbon nanomaterials (e.g., porous carbons, graphene, carbon nanotubes, and so forth) or common pseudocapacitive metal oxides (e.g., MnO₂) where a combination of a carbonyl or multi-electron redox containing compounds boost charge storage performance at low scan rates, likely due to variety of interactions and charge transfer happening at Ti₃C₂T_x MXene and organic interfaces, as noted in the above computational discussion.^[9,18] Of course, further optimization of these hybrid electrodes could be performed in the future.

3. Conclusion

We have synthesized three different multi-electron redox-active organic molecules namely C1 (2-pyridin-1-ium-1-yl-1,4-benzoquinone chloride), C2 (2,5-di(pyridin-1-ium-1-yl)-1,4-benzoquinone chloride), and C3 (1,1-di(1,4-benzoquinonyl)-4,4'-bipyridinium

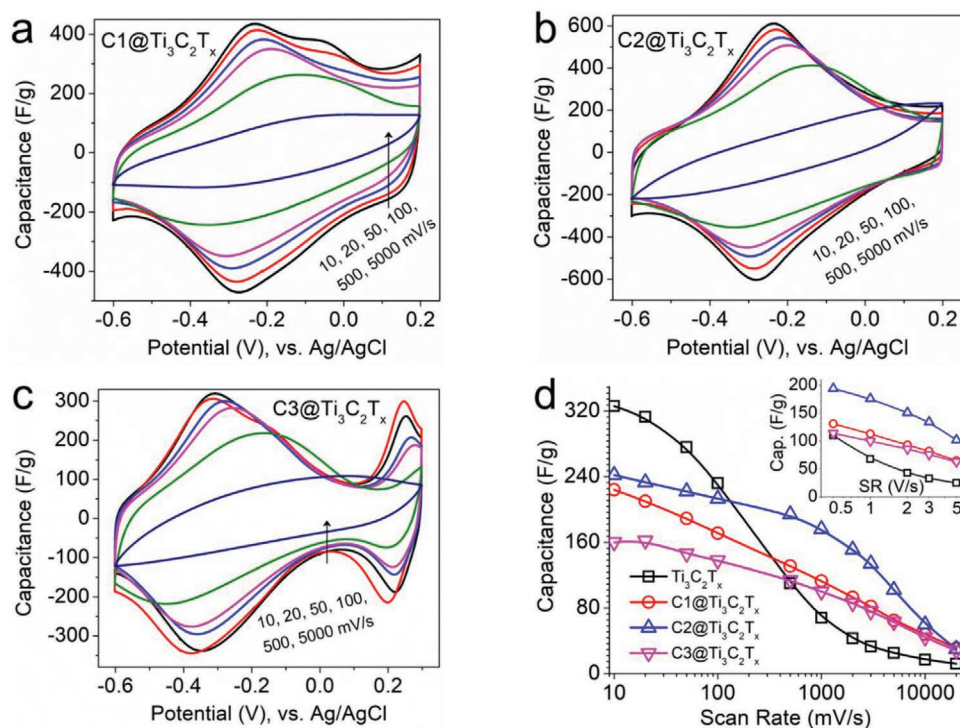


Figure 6. Pseudocapacitive charge storage performance of a) C1@Ti₃C₂T_x, b) C2@Ti₃C₂T_x, c) C3@Ti₃C₂T_x, and d) corresponding rate performance. Inset in (d) magnifies the ultra-high scan rates portion of the plot.

chloride) by simple mixing at room temperature followed by their functionalization on Ti₃C₂T_x MXene using a self-assembly approach. We found that intercalation of these organic molecules was size-dependent, with smaller molecules (C1@Ti₃C₂T_x) showing the highest c-LP expansion of over 20 Å. The PDF analysis showed that the intercalation of organic molecules changes the local structure by adding contributions from organic molecules. Moreover, different organic molecules similarly change the MXene inter-layer structure by removing the residual stacking order that may have existed in the pristine Ti₃C₂T_x MXene. Spectroscopic results confirmed that all molecules functionalized on Ti₃C₂T_x via hydrogen bonding without their catalytic dissociation. We concluded that the hybrids with controlled properties can be designed by introducing functionalities on organic molecules that are less likely to offer catalytic decomposition at the MXene interface. DFT calculations confirmed that molecules preferred to bind horizontally on the MXene surface, involved in charge transfer and, all hybrids preserved their metallic behavior. All hybrids exhibited an improved capacitance at ultra-high scan rates due to molecular pillaring of the organics between MXene layers. These results may guide the synthetic methods to produce next-generation organic@MXene hybrids with controlled properties for a large set of applications.

Supporting Information

Supporting Information is available from the Wiley Online Library or from the author.

Acknowledgements

The authors thank Prof. Yury Gogotsi for guiding this work. This work was supported as part of the Fluid Interface Reactions, Structures and Transport (FIRST) Center, an Energy Frontier Research Center funded by the U.S. Department of Energy, Office of Science, and Office of Basic Energy Sciences. L.Y.'s effort on PDF analysis and modeling was supported by the NSF MRSEC program through Columbia in the Center for Precision Assembly of Superstratic and Superatomic Solids (DMR-1420634). X-ray PDF measurements were conducted on beamline 28-ID-2 of the National Synchrotron Light Source II (NSLS-II), a U.S. Department of Energy (DOE) Office of Science User Facility operated for the DOE Office of Science by Brookhaven National Laboratory under Contract No. DE-SC0012704. R.A. thanks Swedish Research Council (VR-2016-06014) for financial support. SNIC and HPC2N are acknowledged for providing the computing facilities.

Conflict of Interest

The authors declare no conflict of interest.

Data Availability Statement

The data that support the findings of this study are available from the corresponding author upon reasonable request.

Keywords

2D materials, hybrid materials, MXene, redox-active organic materials, supercapacitors, titanium carbide

Received: December 14, 2020

Revised: February 3, 2021

Published online: March 16, 2021

- [1] B. Anasori, M. R. Lukatskaya, Y. Gogotsi, *Nat. Rev. Mater.* **2017**, *2*, 16098.
- [2] Y. Gogotsi, B. Anasori, *ACS Nano* **2019**, *13*, 8491.
- [3] F. Shahzad, M. Alhabeb, C. B. Hatter, B. Anasori, S. Man Hong, C. M. Koo, Y. Gogotsi, *Science* **2016**, *353*, 1137.
- [4] M. R. Lukatskaya, S. Kota, Z. Lin, M.-Q. Zhao, N. Shpigiel, M. D. Levi, J. Halim, P.-L. Taberna, M. W. Barsoum, P. Simon, Y. Gogotsi, *Nat. Energy* **2017**, *6*, 17105.
- [5] D. Wang, F. Li, R. Lian, J. Xu, D. Kan, Y. Liu, G. Chen, Y. Gogotsi, Y. Wei, *ACS Nano* **2019**, *13*, 11078.
- [6] L. Gao, C. Li, W. Huang, S. Mei, H. Lin, Q. Ou, Y. Zhang, J. Guo, F. Zhang, S. Xu, H. Zhang, *Chem. Mater.* **2020**, *32*, 1703.
- [7] O. Mashtalir, M. Naguib, V. N. Mochalin, Y. Dall'Agnese, M. Heon, M. W. Barsoum, Y. Gogotsi, *Nat. Commun.* **2013**, *4*, 1716.
- [8] M. Boota, B. Anasori, C. Voigt, M.-Q. Zhao, M. W. Barsoum, Y. Gogotsi, *Adv. Mater.* **2015**, *28*, 1517.
- [9] M. Boota, C. Chen, L. Yang, A. I. Kolesnikov, N. C. Osti, W. Porzio, L. Barba, J. Jiang, *Chem. Mater.* **2020**, *32*, 7884.
- [10] M. Boota, P. Urbankowski, W. Porzio, L. Barba, N. C. Osti, M. Bleuel, J. K. Keum, E. Mamontov, *ACS Appl. Energy Mater.* **2020**, *3*, 4127.
- [11] M. Boota, M. Pasini, F. Galeotti, W. Porzio, M.-Q. Zhao, J. Halim, Y. Gogotsi, *Chem. Mater.* **2017**, *29*, 2731.
- [12] C. Chen, M. Boota, X. Xie, M. Zhao, B. Anasori, C. E. Ren, L. Miao, J. Jiang, Y. Gogotsi, *J. Mater. Chem. A* **2017**, *5*, 5260.
- [13] G. S. Lee, T. Yun, H. Kim, I. H. Kim, J. Choi, S. H. Lee, H. J. Lee, H. S. Hwang, J. G. Kim, D. Kim, H. M. Lee, C. M. Koo, S. O. Kim, *ACS Nano* **2020**, *14*, 11722.
- [14] S. H. Overbury, A. I. Kolesnikov, G. M. Brown, Z. Zhang, G. S. Nair, R. L. Sacci, R. Lotfi, A. C. T. van Duin, M. Naguib, *J. Am. Chem. Soc.* **2018**, *140*, 10305.
- [15] C. Chen, M. Boota, P. Urbankowski, B. Anasori, L. Miao, J. Jiang, Y. Gogotsi, *J. Mater. Chem. A* **2018**, *6*, 4617.
- [16] T. Nishinaga, *Organic Redox Systems: Synthesis, Properties, and Applications*, John Wiley & Sons, New York / Chichester, UK **2015**.
- [17] S.-E. Chun, B. Evanko, X. Wang, D. Vonlanthen, X. Ji, G. D. Stucky, S. W. Boettcher, *Nat. Commun.* **2015**, *6*, 7818.
- [18] M. Boota, C. Chen, K. L. Van Aken, J. Jiang, Y. Gogotsi, *Nano Energy* **2019**, *65*, 104022.
- [19] T. Egami, S. J. L. Billinge, *Underneath the Bragg Peaks Structural Analysis of Complex Materials*, Elsevier, Amsterdam **2012**.
- [20] P. Urbankowski, B. Anasori, K. Hantanasirisakul, L. Yang, L. Zhang, B. Haines, S. J. May, S. J. L. Billinge, Y. Gogotsi, *Nanoscale* **2017**, *9*, 17722.
- [21] R. B. Neder, V. I. Korsunskiy, *J. Phys.: Condens. Matter.* **2005**, *17*, S125.
- [22] C. A. Young, A. L. Goodwin, *J. Mater. Chem.* **2011**, *21*, 6464.
- [23] C. Shi, M. Beidaghi, M. Naguib, O. Mashtalir, Y. Gogotsi, S. J. L. Billinge, *Phys. Rev. Lett.* **2014**, *112*, 125501.
- [24] W. Zhang, H.-J. Li, Y. Wang, Y. Liu, Q.-Z. Gu, Y.-C. Wu, *New J. Chem.* **2018**, *42*, 12649.
- [25] A. Ben-Refael, I. Benisti, Y. Paz, *Catal. Today* **2020**, *340*, 97.
- [26] N. Davletshina, A. Khabibullina, J. Ushakova, R. Davletshin, D. Islamov, K. Usachev, R. Cherkasov, *J. Organomet. Chem.* **2020**, *916*, 121267.
- [27] X.-L. Wang, Y.-F. Li, C.-L. Gong, T. Ma, F.-C. Yang, *J. Fluorine Chem.* **2008**, *129*, 56.
- [28] C. Y. Panicker, H. T. Varghese, D. Philip, H. I. S. Nogueira, *Spectrochim. Acta, Part A* **2006**, *64*, 744.
- [29] B. Zhang, Y. Zhou, X. Li, X. Ren, H. Nian, Y. Shen, Q. Yun, *Spectrochim. Acta, Part A* **2014**, *122*, 59.
- [30] Y.-Q. Zhang, X.-W. Wei, R. Yu, *Catal. Lett.* **2010**, *135*, 256.
- [31] Q. Sun, W. Wang, C. Zhang, Q. Huang, S. Zhang, *J. Chem. Crystallogr.* **2019**, *50*, 308.
- [32] M. Boota, M. Rajesh, M. Bécuwe, *Mater. Today Energy* **2020**, *18*, 100532.
- [33] M. Boota, K. B. Hatzell, M. Alhabeb, E. C. Kumbur, Y. Gogotsi, *Carbon* **2015**, *92*, 142.
- [34] J. S. Strukl, J. L. Walter, *Spectrochim. Acta, Part A* **1971**, *27*, 209.
- [35] N. V. Blinova, J. Stejskal, M. Trchová, J. Prokeš, M. Omastová, *Eur. Polym. J.* **2007**, *43*, 2331.
- [36] R. Jayan, M. M. Islam, *Nanoscale* **2020**, *12*, 14087.
- [37] C. R. DeBlase, K. E. Silberstein, T.-T. Truong, H. D. Abruña, W. R. Dichtel, *J. Am. Chem. Soc.* **2013**, *135*, 16821.
- [38] C. E. Ren, M. Zhao, T. Makaryan, J. Halim, M. Boota, S. Kota, B. Anasori, M. W. Barsoum, Y. Gogotsi, *ChemElectroChem* **2016**, *3*, 689.
- [39] M. Yao, H. Senoh, S. I. Yamazaki, Z. Siroma, T. Sakai, K. Yasuda, *J. Power Sources* **2010**, *195*, 8336.